Vibrational dynamics and phonon dispersion of polycrystalline ice XII and of high-density amorphous ice

M. M. Koza,[1] H. Schober,[1] S. F. Parker,[2] and J. Peters[1,3,4]
[1]*Institut Laue-Langevin, 6 rue Jules Horowitz, Boite Postale 156, F-38042 Grenoble Cedex 9, France*
[2]*ISIS Facility, Chilton, Didcot Oxon, Oxon OX11 0QX, United Kingdom*
[3]*Universite Joseph Fourier, F-38042 Grenoble Cedex 9, France*
[4]*Institut de Biologie Structurale, F-38042 Grenoble Cedex 9, France*
(Received 2 July 2007; revised manuscript received 17 February 2008; published 27 March 2008)

The dynamics of high-density polycrystalline ice XII have been studied with neutron and x-ray scattering techniques in the range of translational and librational modes. Depending on the energy range of interest, different neutron spectrometers have been utilized. This way, accurate information on mode energies, sound velocities ($\bar{v}=2350\pm50$ m/s), and the Debye temperature ($T_D=240\pm2$ K) have been obtained. Having applied protonated (H_2O) and deuterated (D_2O) sample material, we were as well able to study the effects of coherence on the inelastic response and to follow the dispersion of acoustic phonons in the second Brillouin zone. The purely coherent scattering character and the kinematics of x rays were exploited to follow the dispersion of phonons in the first Brillouin zone, to discriminate between modes of longitudinal and transverse polarizations, and to determine the longitudinal velocity of sound ($v_l=4060\pm50$ m/s). In addition, the inelastic properties of ice XII are compared to the responses of polycrystalline cubic ice I_c and the high-density amorphous structure.

DOI: 10.1103/PhysRevB.77.104306 PACS number(s): 63.20.−e, 61.05.fg, 61.05.cf, 63.50.−x

I. INTRODUCTION

In the recent past, the dynamics of the manifold of crystalline water ice phases have been the focus of extensive experimental work.[1] A considerably detailed study has been performed by incoherent inelastic neutron scattering (IINS).[2–7] The virtue of the IINS technique lies within its experimental response giving access to the vibrational density of states $G(\omega)$ of a sample. $G(\omega)$ is determined by the force constant distribution, i.e., the second derivatives of the atomic potential of the samples' constituents. It is hence an observable which sensitively reflects the details of atomic and molecular arrangements in a sample and serves as a highly accurate probe for potentials used in computer calculations.

Unlike other molecular crystals, water ice structures are, in principle, an extraordinarily favorable case for such a complementary study. Due to the difference of intra- and intermolecular bond energies, the eigenmodes of the ice structures are well separated in energy. They form bands of pure phononic (translational excitations of the entire molecule), librational (hindered rotations of molecules), and intramolecular vibrational (bending and stretching of a molecule) character. Hence, the effect of crystal symmetry and of density variations can be studied on any of the eigenmode bands with high accuracy.

The diversity of ice structures of different density is due to two compacting strategies. On the one hand, the weak H bonds allow an extensive variation of bonding angles departing from the tetragonal angle of ordinary ice I_h. This is accomplished at moderate pressures in ice structures II, III/IX, IV, and V.[1,8] On the other hand, at pressures above 1 GPa, the presence of wide water rings allows a partial interpenetration of these rings like in ice VI or a self-clathration of two fully bonded and independent ice matrices like in ice VII and VIII.

Among these many ice phases, ice XII ($I\bar{4}2d$) (Refs. 9 and 10) shows some structural peculiarities which should be uniquely reflected in its inelastic response. It is one of the non-self-clathrating and non-interpenetrating ice structures with highest mass density ($\rho=43$ molecules/nm^3). The structure of ice XII is composed of seven- and eight-membered rings, "… and is the first example of a four-connected network of this type."[10] However, so far, apart from coherent inelastic neutron scattering,[11] inelastic x-ray scattering,[12] and Raman scattering experiments sensitive to a set of Γ-point vibrations,[13,14] a comprehensive study of the microscopic collective dynamics of ice XII is missing.

In this paper, we report on extensive experimental results designed to shed some light on the features in the phonon and librational band of ice XII. Our experiments do not only fall into line with previous IINS studies performed on other crystalline ice structures,[3–7] but they also amplify the observations to very high-resolution neutron spectroscopy, inelastic x-ray scattering (IXS), and coherent inelastic neutron scattering (CINS). The present paper is purely based on experimental work and focuses on the establishment of inelastic properties of ice XII in the energy range $\hbar\omega\leqslant150$ meV.

For the readers' convenience, after introducing the experimental setups and the sample preparation, we will present in some detail the experimental characterization of the crystalline phase ice XII and the high-density amorphous ice. The results are structured into a description of the IINS results, a discussion of coherence effects in the signal measured by CINS, followed by an inspection of the applicability of the Debye model of harmonic solids based on the derived velocities of sound and Debye temperatures. We will compare the CINS results with purely coherent IXS data and finish by summarizing on the most important results.

II. EXPERIMENT

A. Instrumentation

The neutron spectrometers TOSCA@ISIS, IN6@ILL, IN13@ILL, and the x-ray inelastic beamline ID28@ESRF were chosen for our studies. These spectrometers complement each other in terms of sampling of the energy momentum phase space and their excellent energy resolution properties.

TOSCA@ISIS, situated at a thermally moderated beam, is an inverse time-of-flight spectrometer. It is fed with a polychromatic neutron beam from the ISIS spallation source at the Rutherford Appleton Laboratories in Didcot, UK. After the scattering process, the energy distribution is determined by a monochromator analyzer with a relative energy resolution of about 2%. It exploits the Stokes line, i.e., the energy loss of neutrons, of the scattering process, enabling the sampling of energies of up to 1000 meV with a sample being kept at 20 K.

IN6@ILL is a direct time-of-flight neutron spectrometer positioned at a cold-neutron guide of the European neutron source Institut Laue Langevin, Grenoble, France. The peculiarity of this spectrometer is the monochromatization of the incoming neutron beam with a crystal monochromator array. In the case of the so-called inelastic time-focusing mode, the relative energy resolution can be set to 2% with the focus of best energy resolution on the range of interest. We have used IN6@ILL with an incident neutron wavelength of 4.14 Å and the focus of best energy resolution (150 μeV) set to about 8 meV, hence, around the energy at which strong inelastic intensity is observed in ice structures.[1] IN6@ILL exploits the anti-Stokes line of scattering processes.

IN13@ILL is a thermal backscattering spectrometer designed for best energy resolution in a wide range of Q-momentum space. Its energy resolution is 8 μeV spanning a Q range up to 4.9 Å^{-1}. The data presented have been collected with the elastic scan mode allowing us to determine the Debye-Waller factor and hence the mean-square displacement of the structures, a subsidiary measure to the low-energy density of states determined at IN6@ILL.[15,16]

ID28@ESRF is an x-ray spectrometer situated at the European Synchrotron Radiation Facility in Grenoble, France. The excellent energy resolution of about 1.5 meV is accomplished by crystal monochromators and crystal analyzers utilized in backscattering geometry. Due to the purely coherent scattering character of x rays, we have exploited ID28@ESRF to gain information on collective phonon modes with a particular focus on the first reduced Brillouin zone and its zone boundary of the crystalline structures.[17] In the case of neutrons, this low Q range is hardly accessible owing to the kinematic properties of the probe.

B. Sample preparation and characterization of phases

All samples were formed at low temperatures ($T \approx 77$ K) and a maximum pressure of 18 kbar in a piston cylinder apparatus. Ice XII samples were prepared by rapid compression of hexagonal ice I_h.[18] Protonated (H_2O, millipore grade) and deuterated (D_2O, 99.8% purity) samples were prepared. High-density amorphous (HDA) ice was measured for comparison. HDA was formed from ice I_h at 77 K and a maximum pressure of 18 kbar by slow compression.[19] Table I presents an overview on the samples studied at the different spectrometers.

TABLE I. Definition of ice XII and HDA samples and instruments at which they have been studied.

	TOSCA	IN6	IN13	ID28
H_2O ice XII	1	4+7	7	8
D_2O ice XII	2	5		
D_2O HDA	3	6		

The formed high-density structures were recovered from the pressure cell and coarsely ground at ambient pressure in liquid nitrogen. As far as ice XII is concerned, its polycrystalline constitution is an intrinsic feature of the samples and not created by the grinding. Closed cycle refrigerators were used for the experiments at TOSCA@ISIS and ID28@ESRF; standard cryostats were utilized at IN6@ILL and IN13@ILL. Aluminum sample holders were used for the neutron scattering experiments; the x-ray experiment was performed in an open-window sample holder described in Ref. 20. Except for inducing the transformation of ice XII into ice I_c reported below, the measurement temperatures with ice XII were 20 K (TOSCA@ISIS), 100 K (IN6@ILL), and 70 K (ID28@ESRF). The experiments performed at IN13@ILL were carried out on stepwise heating with an equivalent heating rate of 10 K/h. The response of HDA sample 6 was measured at 75 K at IN6@ILL, and the one of sample 3 was studied at 20 K at TOSCA@ISIS.

A particular concern in our experimental approach was the quality of the samples and the purity of the structures. As far as coherent scattering can be exploited, the static structure factor $S(Q)$ gives a direct measure of the sample structure and constitution. This was the case in the IXS experiment at ID28@ESRF, whereby the diffraction profile of the sample has already been reported in Ref. 12.

The nuclear scattering of neutrons comprises both coherent and incoherent contributions, governed by an isotope dependent cross section. Table II gives an overview of the relevant nuclear scattering cross sections.

In the case of deuterated samples, the predominant coherent signal allows the sampling of $S(Q)$. Figure 1 reports the $S(Q)=\int S(Q,\omega)d\omega$ of the deuterated ice XII and HDA samples 5 and 6 measured at IN6@ILL.

Within the accuracy of the measurements, the samples are free of any other structures than those to be studied. In the case of protonated samples, i.e., for predominantly incoherent scattering, there is no information on the static correla-

TABLE II. Nuclear scattering cross sections in barn $=10^{-24}$ cm^{-2} (Ref. 21).

	H	D	O	H_2O	D_2O
σ_{coh}	1.76	5.59	4.23	7.75	15.41
σ_{inc}	80.27	2.05	0.00	160.54	4.10

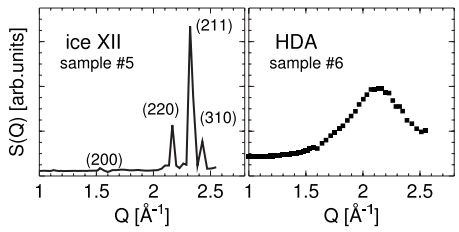

FIG. 1. Static structure factor of deuterated crystalline ice XII and high-density amorphous ice (samples 5 and 6) measured with λ_i=4.14 Å at IN6@ILL.

tions. The quality of the samples and purity of the phases were checked by their transition behavior and their specific inelastic response when compared to their deuterated counterparts.

HDA and ice XII reveal different transition scenarios. HDA transforms via a low-density amorphous (LDA) ice structure into a crystalline cubic modification, ice I_c.[22] The amorphous-amorphous transformation has been observed to start at temperatures as low as 80–85 K.[23,24] Whereby not only the static structure factor but also the inelastic response change visibly.[2,25,26] Ice XII, on the other hand, directly transforms into ice I_c at temperatures above 125 K,[11,27,28] i.e., at a temperature at which all high-density amorphous structures so far produced have ceased to exist.[22–24,26,28,29] An ice XII sample on transformation also displays a strong modification of the dynamic properties whose onset can be interpreted as the temperature of transition T_c.[11] However, since the transformation is a kinetic process, the exact transition temperatures depend, to a certain degree, on the heat treatment of the sample. Hence, slow annealing experiments at constant temperature lead to lower T_c than experiments based on heating with a constant heating rate.

Figure 2 reports on the differences in the inelastic response as obtained with samples 1 and 4 at TOSCA@ISIS and IN6@ILL, respectively. Sample 1 was gradually heated with ΔT=5 K and the temperature was kept constant for long periods after each temperature step. Changes of the signal due to a transformation are not visible until the sample is

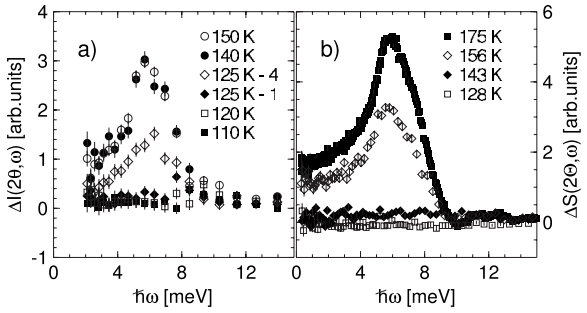

FIG. 2. Difference in inelastic intensity observed during the heating of protonated ice XII samples 1 and 4 plotted in (a) and (b), respectively. Temperatures at which sample 1 was held at least 2 h are given in (a). The onset of the transformation of ice XII into ice I_c can be clearly identified at $T \approx 125$ K, at which about 50% of ice I_c is formed after 6 h. The onset of the transformation in sample 4 can be identified at T=156 K.

kept for 6 h at 125 K. Consequently, the presence of HDA in the sample can be unequivocally excluded and only ice XII is present.

Sample 4 was heated with a constant heating rate of about 1 K/min. Here, the changes are visible at temperatures above 145 K. As we will show later, a T_c of 145 K can be estimated from the IN13@ILL experiment with sample 7. In conclusion, the overall behavior of T_c corresponds well to established data[27] leaving no doubt about the initial phases being pure ice XII structures.

C. Data processing

Basic corrections have been performed to all neutron scattering data comprising subtraction of empty holder scattering, suppression of malfunctioning detectors, and calibration of detectors to an incoherent standard. For calibration purposes, either the intensity of a vanadium standard or of the incoherently scattering solid H_2O sample was applied. In the case of IXS, no empty sample holder measurement was needed due to the sample holder design optimized for the scattering geometry of the ID28@ESRF instrument. In addition, IN6@ILL data were corrected for a weak frame overlap effect.

For samples 4 and 5, additional measurements at a temperature of 1.7 K were performed. Those data serve to suppress the elastic line contribution from the signal monitored at 100 K. This way, the most accurate information on the inelastic intensity in the low-energy region ($\hbar\omega < 2$ meV) can be obtained. Such an approach is, however, only reliably applicable to the anti-Stokes line of the spectra, i.e., the IN6@ILL results.

In this paper, all observables presented are obtained from the corrected data by having applied established mathematical expressions.[30,31] The generalized density of states $G(\omega)$ has been calculated in the incoherent approximation taking into account the entire phase space sampled by the respective instrument. It has been normalized to 12 phonon modes in the energy range of up to 40 meV. This normalization follows our previous data processing accounting for three phonon modes of four molecules in a unit cell of hexagonal ice I_h.[16,25] $G(\omega)$ of ice XII may be, hence, directly compared to our prior publications.

The discussion of the phonon dispersion is based on constant Q data. Here, the CINS dynamic structure factor had to be interpolated from constant 2Θ to constant Q slices, i.e., from $S(2\Theta,\omega)$ to $S(Q,\omega)$. An equidistant Q binning was chosen with ΔQ=0.025 Å^{-1}. To a very high accuracy, constant Q spectra are the natural slicing procedure of the IXS technique. A ΔQ=0.15 Å^{-1} was chosen.

III. RESULTS AND DISCUSSION

A. Incoherent inelastic response of ice XII

Figures 3 and 4 report the dynamic structure factor of ice XII in comparison to ice I_c recorded at TOSCA@ISIS. As is indicated in the figures, Fig. 3 displays the signal of translational vibrations of the molecules (phonons) and of molecular librations, both separated by a mode gap. Figure 4 dis-

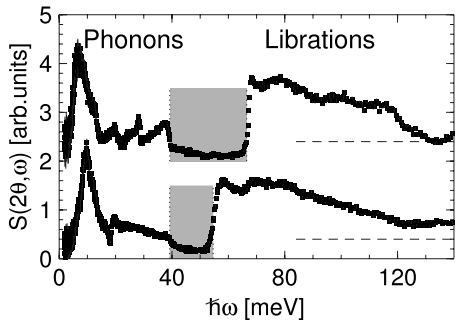

FIG. 3. Incoherent dynamic structure factor $S(2\Theta,\omega)$ of ice XII (bottom) and ice I_c (top) in the energy range of phonons and molecular librations. The gray shaded area marks the energy gap which separates the phonon bands, extending up to 40 meV in both phases, and the librations, setting in at 54 meV in ice XII and 67 meV in ice I_c. The horizontal, dashed line represents the background observed at higher energies (Fig. 4) in the sample.

plays the inelastic response extended up to the energies of the intramolecular bending and stretching modes around 200 and 400 meV, respectively.

The phonon regime $0 \leqslant \hbar\omega \leqslant 40$ meV of the ice XII spectrum shows a predominant, characteristic strong peak centered at about 10 meV, which is also observed in other nonself-clathrating ice phases II, III/IX, V, as well as ice VI. It is accordingly shifted to higher energies than in ice I_c. This accordance equally holds for the shift of the librational band toward lower energies, setting in at about 54 meV. The peculiarity of the ice XII response is the pronounced homogeneous distribution of modes in the phonon energy range of 20–40 meV and the librational band.

In contrast to the phonon part, there is a visible background underneath the intramolecular modes starting at the high-energy edge of the librational band. This background is due to contributions from multi-inelastic neutron scattering events, comprising, e.g., phonon-libration, libration-libration, libration-bending, bending-bending, etc., combinations of events. The multi-inelastic effects are best seen in the response of ice I_c at energies around 300 meV, where a broad peak is detected, although it has been well established that this range is a mode free regime.[5,7] This broad peak is due to libration-bending double scattering. The rather uniform signal in ice XII in Fig. 4 is caused by the shift of the librational band toward lower energies, allowing for multi-inelastic scattering events that fit well between the mode peaks. For example, libration-libration events are accountable for filling up the intensity in the energy range between librational and bending modes.

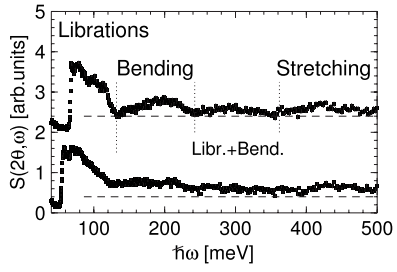

FIG. 4. Incoherent dynamic structure factor $S(2\Theta,\omega)$ of ice XII (bottom) and ice I_c (top) in the energy range of molecular librations and intramolecular bending and stretching modes. The horizontal, dashed line represents the background which is qualitatively estimated from the response of ice I_c. Details are given in the text.

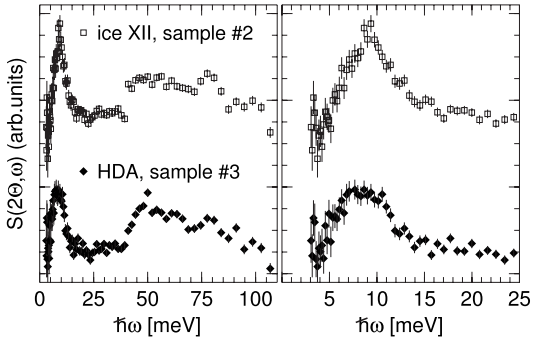

FIG. 5. Coherent dynamic structure factor $S(2\Theta,\omega)$ of ice XII sample 2 (top) and HDA (bottom) sample 3. Left: the energy range of phonons and molecular librations is reported. Right: the strong maximum in the acoustic region of phonons. The ice XII signal is shifted for clarity.

To finalize the discussion of the experiments at TOSCA@ISIS, we present in Fig. 5 the inelastic response of the deuterated ice XII and HDA samples 2 and 3. The higher mass and momentum of inertia of the D_2O molecules have two visible effects on the librational band. On the one hand, the entire band is shifted toward lower energies by about 15 meV. On the other hand, the momentum of inertia reduces the effective intensity of the librational band relative to the intensity of the phonons.[32,33] Despite the relaxed statistics, there is an indication that the low-energy edge of the librational band is sharper in ice XII compared to HDA. However, higher quality experiments are necessary to confirm this apparent tendency.

When comparing the translational excitations on the right hand side of Fig. 5, a clear difference in the position and width of the strong maxima can be detected. The ice XII peak is centered at higher energy and is sharper than the HDA maximum. However, for obtaining the most accurate information in this energy range, the cold-neutron spectrometer IN6@ILL is best suited.

Figure 6 reports the generalized density of states $G(\omega)$ of ice XII as is monitored in the entire momentum range of IN6@ILL. Figure 6(a) shows $G(\omega)$ of the protonated and deuterated samples 4 and 5, Figure 6(b) compares the $G(\omega)$ of deuterated samples ice XII 5 and HDA 6. Apart from a slight shift of $G(\omega)$ of the deuterated sample toward low energies, which is due to the molecular mass effect $\hbar\omega \sim 1/\sqrt{M}$, identical features are present in both ice XII samples.

As far as ice I_h is concerned, its intense low-energy peak is determined by acoustic and, in particular, two optic modes of transverse polarization.[5,34,35] The presence of such low-energy optic modes has been also confirmed in ice XII as well as ice IX by IXS.[12] A clear separation of eigenmodes into acoustic and optic bands is therefore not appropriate in ice XII either. We will show later that a dispersive maximum

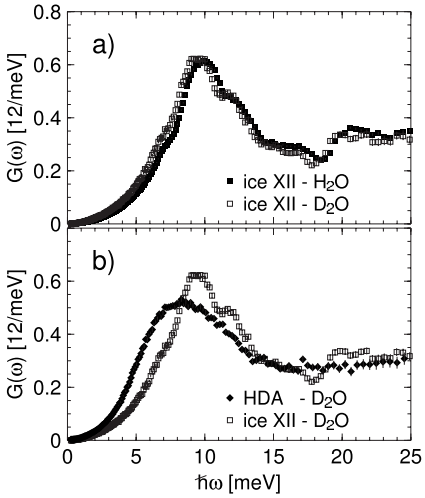

FIG. 6. Generalized density of states $G(\omega)$ of protonated (full squares, sample 4) and deuterated (empty squares, sample 5) ice XII, and high-density amorphous ice (full diamonds, sample 6) measured with λ_i=4.14 Å^{-1} at IN6@ILL. All $G(\omega)$ are normalized to 12 phonon modes in accordance with prior publications on ice I_h and I_c.

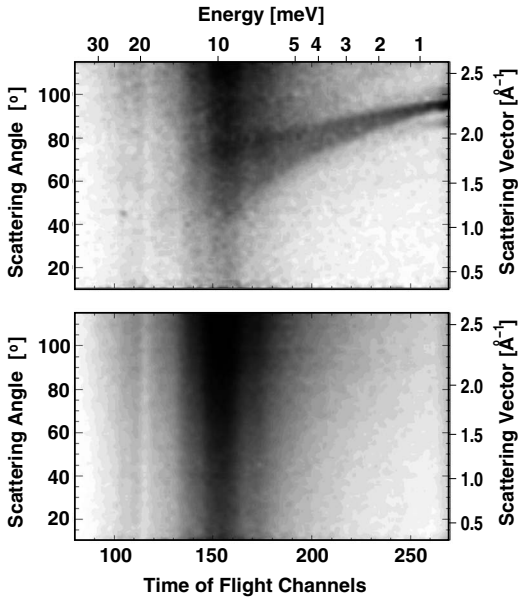

FIG. 7. Contrast plot of the inelastic intensity measured at IN6@ILL with deuterated (top) and protonated (bottom) samples 5 and 4. Here, the scattering angle and the time-of-flight channels are the natural units of the experiment. Energy and scattering vector values are given for reason of comprehensibility. Values of the scattering vector are only valid for the elastic line of the spectra. The elastic line displaying the static correlations of the samples is centered at the time-of-flight channel 282, i.e., outside the displayed time-of-flight window.

can be followed up to an energy of about 24 meV and, hence, a classification of phonons according to their dispersion is more complex in detail.

When taking the $G(\omega)$ of HDA into consideration, it is obvious that such distinct features are missing. Besides the strong peak, which can also be identified as due to low-energy transverse optic modes,[12,20] the inelastic response appears to be smoothed out throughout the entire energy range. This equally holds for amorphous ice structures of even higher density and most of the structures occurring in the course of the transformation of HDA into a low-density modification.[25,26] To a certain extent, HDA's rather untextured $G(\omega)$ resembles the response of liquid water whose characteristics are a broad maximum in the range of translational excitations around 8 meV and the librational band shifted toward lower energies of 50 meV.[36]

B. Coherence effects in the low-energy response and the incoherent approximation

Figure 7 presents an overview of the inelastic intensity of the deuterated (top) and the protonated (bottom) ice XII samples 5 and 4 measured at IN6@ILL. The data are plotted in natural units of the experiment, i.e., the x axis corresponds to the time of flight given as channel number (1 channel =11.75 μs), and the y axis corresponds to the scattering angle. Please note that the x axis is inverted since a shorter time of flight of neutrons corresponds to higher energies of the annihilated phonon modes of the anti-Stokes line. In the contrast plots of Fig. 7, features of higher intensity appear darker in color. Features common to both samples obviously become more intense toward higher scattering angles. In the most simple scenario of pure incoherent scattering, we may assume that it is due to the $\propto Q^2$ dependence of the incoherent scattering intensity.[30,31]

The strong dispersive band and the two weaker side bands observed toward longer time of flight in the deuterated sample are due to acoustic phonons. They are only detectable in the presence of predominantly coherent scatterers. Their originating points are the strong Bragg reflections [(220), (211), (310)] at 0 meV reported in Fig. 1. Despite the valuable information, one gains on the lattice dynamics and, thus, the material properties of the sample by the detection of the dispersion relation of acoustic excitations; the computation of thermodynamic properties via the Debye model $G(\omega)/\omega^2$ is *a priori* made more difficult, since the low-energy part of $G(\omega)/\omega^2$ is visibly obscured.

This apparent obstacle, however, can be elegantly bypassed by extracting $G(\omega)$ from a subrange of the Q-ω phase space, which is free from strong coherent signal due to acoustic phonons. When taking data only in the range $2\Theta \geqslant 105°$ into consideration, the intensity of the Debye level is determined by the incoherent cross section of the deuterated sample 1. Figure 8 demonstrates the effect on the Debye level of the deuterated sample as is calculated for the complete and a reduced phase space. $G(\omega)/\omega^2$ calculated from the reduced data set matches well the signal of the purely incoherent scatterer, which reflects best the true density of states. Energies of van Hove singularities [peaks at about 7 and 9 meV in the $G(\omega)/\omega^2$ presentation] are unaffected by this procedure since they uniquely depend on the mass of the scatterers and not on the scattering character, coherent or incoherent. However, it is also clear from Fig. 8 that such a data treatment results in a reduced statistical accuracy, due to

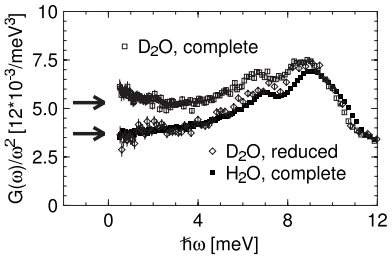

FIG. 8. Generalized density of states $G(\omega)$ of protonated (full squares) and deuterated (empty squares, empty diamonds) ice XII samples normalized to 12 phonon modes and scaled by ω^2 according to the Debye model. Full squares and empty squares represent the information obtained from the complete phase space accessed in the scattering experiment (Fig. 6). Empty diamonds are calculated from data detected at $2\Theta \geqslant 105°$ at which the signal from acoustic phonons is strongly suppressed. Horizontal arrows indicate the estimated Debye levels for the two samples.

the reduced phase space as well as to the small incoherent cross section of D_2O.

When trying to extract a factor X for a scaling of the complete coherent $G(\omega)/\omega^2$ onto the incoherent signal in the Debye regime, we obtain $X \approx 0.7$. This factor agrees well with the results concluded on hexagonal and cubic ice structures reported in Ref. 16. The good correspondence of the Debye levels of the protonated with the deuterated samples is also in agreement with findings on ice I_h and the high-density and low-density amorphous ice structures. However, the factor of 0.7 must not be understood as a universal scaling constant but it depends on the sample and the experimental setup. The present case, in which acoustic phonons are only sampled over the second reduced Brillouin zone, is not a favorable scenario.[37–39] Any extension of the monitored phase space toward higher momentum transfers should improve the accuracy and raise the factor X toward unity.

Nonetheless, apart from the very low-energy acoustic region, the general features such as mode energies and intensities are accurately reproduced in the CINS measurements as is demonstrated in Fig. 6. Hence, in the case of water ice, the time-of-flight CINS experiments lead to an excellent incoherent approximation matching the IINS results.

C. Debye model and the mean-square displacement $\langle u^2(T) \rangle$

Complementary information on the properties of structural excitations can be experimentally obtained from monitoring the temperature dependence of the Debye–Waller factor and, hence, of the mean-square displacements $\langle u^2(T) \rangle$.[16] For the crystalline structures ice XII and I_c, we expect the Debye theory of harmonic crystals to be valid given the low temperatures exploited.[40] From this theory, the characteristics of $\langle u^2(T) \rangle$, on the one hand, and of $G(\omega)$ in the regime of acoustic phonons, on the other hand, are determined by a single parameter, the so-called Debye temperature T_D, which is directly related to the average velocity of sound $\bar{v}$.

Figure 9 reports the $\langle u^2(T) \rangle$ of ice XII and I_c obtained with sample 7 at IN13@ILL. Note that the data sets were normalized to the respective data taken at the lowest temperature canceling out the zero point oscillations.[16] $G(\omega)$ of the structures measured at IN6@ILL with a second portion of the same sample are plotted in the insets. Full lines indicate fits of the Debye model to the $\langle u^2(T) \rangle$ data, and the obtained T_D are summarized with data from Ref. 16 in Table III. Around 145 K in the ice XII results of Fig. 9, a step indicates the transition to ice I_c. The upturn of the data reflects the lower velocity of sound and the redshift of the strong maximum in the density of states of ice I_c.

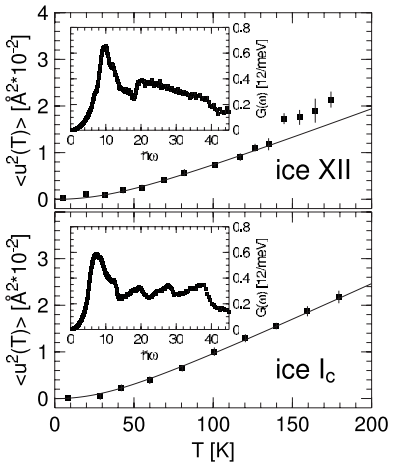

FIG. 9. Mean-square displacement $\langle u^2(T) \rangle$ of sample 7 measured at IN13@ILL. Top figure reports the $\langle u^2(T) \rangle$ of ice XII. The step in the data points at 145 K indicates the transition into ice I_c. Bottom figure reports the $\langle u^2(T) \rangle$ of ice I_c. The insets indicate the corresponding $G(\omega)$ determined with a second portion of sample 7 at IN6@ILL. Full lines correspond to fits of the experimental $\langle u^2(T) \rangle$ following the Debye model of harmonic crystals.

Approximating the density of ice XII by 43 molecules/nm^3, we calculate the averaged velocity of sound to $\bar{v} = 2300 \pm 20$ m/s. This value corresponds well to $\bar{v} = 2350 \pm 50$ m/s ($T_D = 245 \pm 5$ K) determined by the Debye level indicated in Fig. 8. Taking into account the longitudinal velocity of sound of $v_l = 4060 \pm 50$ m/s which has been concluded from IXS experiments,[12] a rough estimation of the transverse velocity of $v_t = 2100 \pm 25$ m/s can be given. In Table IV, these values are compared to the velocity of sound of other crystalline structures determined by the Brillouin light scattering.[41,42] We have chosen values extrapolated to 0 kbar pressure as they are evaluated and given in Ref. 41.

D. Coherent scattering and the dispersion of acoustic phonons

More fundamental information on the velocity of sound and material properties of a sample is given by the dispersion

TABLE III. Debye temperatures T_D obtained for different ice structures from fits of the Debye model to $\langle u^2(T) \rangle$.

	Ice XII	Ice I_c	HDA[a]	LDA[a]	Ice I_c[a]
T_D (K)	240 ± 2	216 ± 3	230 ± 6	217 ± 2	224 ± 7

[a]Data taken from Ref. 16.

TABLE IV. Comparison of the velocity of sound of ice XII with other crystalline ice structures measured by the Brillouin light scattering (Ref. 41).

Phase	v_l	v_t	$\bar{v}$
I_h	3970	1960	2200
II	4320	2090	2340
III/IV	3460	1510	1700
V	4108	2200	2450
VI	4190	1990	2240
XII	4060	2100	2300/2350

of acoustic phonons detectable by coherent scattering. However, the interpretation of the recorded coherent signal is made difficult by two attributes of the experiments. First of all, due to the powder character of the ice XII structures, the CINS experiment monitors properties dependent on the modulus of the momentum Q. In addition, the intensities of phonons are subject to complex selection rules in coherent scattering experiments. These rules apply to the coherent dynamic structure factor $S(Q,\omega)$ and are therefore valid irrespective of the techniques exploited, IXS or CINS.[48] Consequently, $S(Q,\omega)$ constitutes a response which is not only averaged over the space dimensions but also weighted by the underlying selection rules.

In Ref. 12, we have introduced and discussed $S(Q,\omega)$ as was recorded by IXS in the first reduced Brillouin zone (BZ) of ice XII sample 8. Here, we extend the presentation in Fig. 10 to the signal in the vicinity of the second BZ boundary with respect to the (211) Bragg reflection at $Q \approx 2.325$ Å^{-1}, i.e., into the Q range 1.1–1.55 Å^{-1}.

To stay consistent with the data evaluation presented in Refs. 12 and 20, the spectra have been decomposed into three Lorentzian lines. Strictly speaking, this approach is not correct in detail since Lorentzians cannot properly account for the rather sharp intensity cutoff at 40 meV. However, a significant model dependent deviation of the line positions and widths obtained as fit parameters could not be observed. A parametrization of the response with three Gaussians did not result in better numerical accuracy.

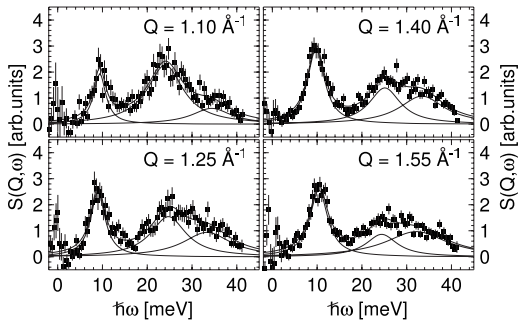

FIG. 10. Coherent dynamic structure factor $S(Q,\omega)$ of sample 8 measured at constant Q with inelastic x-ray scattering on ID28@ESRF. Q values are given in the subfigures. Solid lines correspond with fit results obtained by decomposing the spectral shape into the three Lorentzians. Details are given in the text.

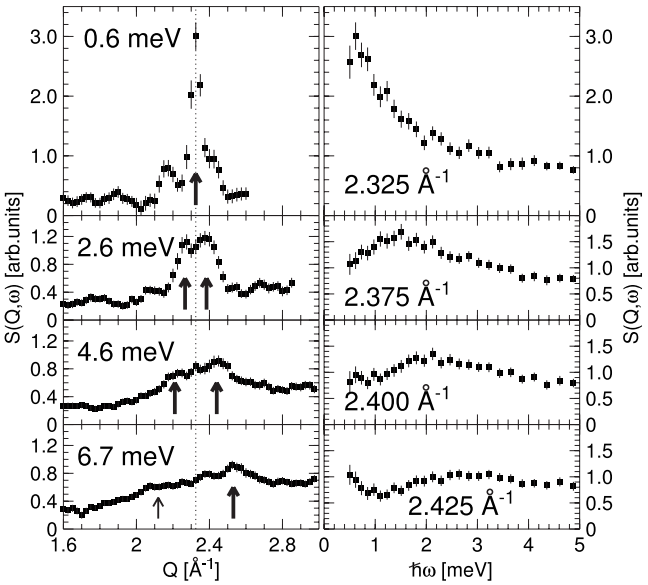

FIG. 11. On the left, selected constant energy spectra $S(Q,\omega)$ and on the right, constant Q spectra of deuterated ice XII sample 5. Energies and Q numbers are indicated in the figures. The energy binning is kept constant as 0.35 meV, i.e., twice the energy resolution of the chosen experimental setup. The Q binning corresponds to 0.025 Å^{-1}. Vertical arrows indicate the identified acoustic phonon, whose dispersion is reported in Fig. 12.

There are two important conclusions that can be drawn from the IXS experiments. On the one hand, the strong peak at 9–10 meV is dominated by optic modes of transverse polarization as can be judged from the weak dispersive character $\hbar\omega(Q)$ and the onset of the mode's intensity close to the zone boundary. On the other hand, a dispersive peak which originates from 0 meV at 0 Å^{-1} can be easily followed up to about 24 meV at the zone boundary shown in Fig. 10. This behavior indicates that the eigenvector of this mode remains rather unaltered throughout the first BZ and the mode can be classified as longitudinal acoustic (LA).

Figure 11 reports on the left hand side constant energy slices from CINS measurements. On top of the incoherent contribution which smoothly ascends toward higher Q numbers, there is a coherent signal of the collective phonon modes which forms a maximum around 2.325 Å^{-1}. With increasing energy, this maximum splits into two peaks which obviously disperse remaining rather symmetrically distributed around 2.325 Å^{-1} which is indicated by the vertical arrows. With respect to the (211) Bragg reflection, these features correspond to acoustic phonons dispersing in the second BZ of the crystal. In the constant Q presentation on the right hand side, a rather broad dispersing maximum is detected whose width can be attributed to the average character of the signal in respect to the three acoustic phonon sheets.

Mode peaks identified in the IXS and CINS experiments are indicated in Fig. 12, whereby translational invariance has been exploited for the presentation of the CINS data. Due to the phonon selection rules, the intensity of the IXS experiment toward low Q numbers is due to a LA mode. The good

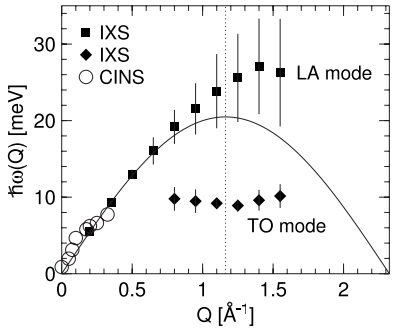

FIG. 12. Dispersion relation $\hbar\omega(Q)$ of the phonon modes of ice XII identified with coherent inelastic neutron scattering (CINS) and inelastic x-ray scattering (IXS). Solid lines with data points represent the mode widths as obtained from fits to constant Q scans (Fig. 12) by IXS. The CINS data are measured within the second Brillouin zone and plotted here applying the principle of translational invariance. Dotted line indicates the reduced (211) BZ boundary and the full line represents an idealized dispersion of the averaged LA phonon.

correspondence of the CINS with the IXS data indicates that the most distinct feature in the powder averaged inelastic intensity is given by the LA mode also within the second BZ. This holds well for $Q>2.325$ Å^{-1}, however, to a lower degree for $Q<2.325$ Å^{-1}, where a clear assignment of a peak to the LA mode is not possible above about 5 meV. For example, following symmetry arguments, a peak at the Q number indicated by the small vertical arrow at 6.7 meV of Fig. 11 should be expected. Within the accuracy of data evaluation, the dispersion relations of the TO and LA modes appear to be rather symmetrical in respect to the $Q=1.1625$ Å^{-1}, i.e., the zone boundary of the $[2\xi\xi\xi]$ direction indicated by the dotted line in Fig. 12. The LA dispersion has been approximated by a sinusoidal function taking only IXS data at $Q<0.5$ Å^{-1} into account.

The LA mode apparently crosses in the powder averaged experiment, some low-energy optic phonon branches without being visibly perturbed. Such an experimental finding can only be resolved by concluding that in the real three-dimensional crystal, the LA phonon sheet interacts, if at all, only weakly with any optic mode of identical polarization in the $[2\xi\xi\xi]$ direction. In other words, its dynamical matrix elements are featured by small values. A possible implication could be that longitudinal optic phonons are highly dispersive to suppress the crossing with the LA $[2\xi\xi\xi]$ phonon branch. Such a feature is well established in ice I_h.[5,34]

IV. CONCLUSIONS

In this paper, we have reported on extensive neutron and x-ray scattering experiments dedicated to the study of the dynamics of ice XII in the range of translational ($0 \leqslant 40$ meV) and librational ($55 \leqslant 120$ meV) modes. Having applied IINS, we have determined the vibrational density of states of ice XII and identified the characteristic features in its profile. In particular, we have accurately established differences in the dynamics of ice XII and the HDA counterpart.

Ice XII reveals a strong sharp peak centered at 10.0 meV in H_2O and 9.5 meV in D_2O polycrystals. This peak is flanked on both sides by a well distinguished shoulder at 7 meV and a smaller peak at 12 meV, respectively, followed by a characteristic intensity dip around 19 meV in H_2O and 18 meV in D_2O. Up to the upper phonon limit of about 40 meV, the density of states shows a rather untextured descending profile. As far as $G(\omega)$ of HDA is concerned, it is untextured in the entire phonon range. The only characteristic feature is a broad maximum with a center redshifted toward 8–9 meV.

On the basis of the Debye model of harmonic crystals, we could approximate the average velocity of sound $\bar{v}$ and the Debye-temperature T_D as 2350 m/s and 340 K, respectively. Purely coherent IXS enabled the estimation of the longitudinal velocity of sound as $v_l=4060$ m/s. IXS was equally helpful to identify the origin of the strong peak around 10 meV as being due to a dominant contribution from optic modes of transverse polarization. On the other hand, it could be confirmed that the longitudinal acoustic phonon branch $[2\xi\xi\xi]$ reaches energies as high as 24 meV.

A detailed discussion of the effect of CINS on an averaged response such as $G(\omega)$ was given. We have shown that time-of-flight experiments sampling the inelastic response of polycrystalline and amorphous ice samples over two Brillouin zones are sufficient to obtain accurate information on general features such as mode energies and intensities in $G(\omega)$. This so-called incoherent approximation is less reliable when properties are concluded from the low-energy part of $G(\omega)$ which is exclusively dominated by acoustic phonons. This point was demonstrated on the variation of the Debye level intensity $[G(\omega)/\omega^2]$ that could have been extracted from IINS and CINS experiments.

We have undertaken considerable efforts to confirm the high quality of the samples and the purity of the phases studied. Our concern originates from the obstacle of forming clean amorphous HDA structures as had been reported in the literature.[25,43–45] Since the structure of a sample studied by IINS cannot be monitored, a quality check of sample material is an issue in IINS experiments unless the inelastic response of ice XII and HDA has been unequivocally established. In the present paper, this goal has been achieved to a high accuracy in the energy range of phonons and librations. The conformity of the inelastic responses in the range of phonons $0 \leqslant \hbar\omega \leqslant 40$ meV determined by IINS and CINS experiments and the simultaneous monitoring of the static structure factor in CINS measurements contribute to the unequivocal identification and assignment of the ice XII and HDA inelastic responses.

The entire body of our IINS, CINS, and IXS results gives evidence of an remarkably untextured $G(\omega)$ of HDA and of other high-density amorphous structures[16,25,26] being reminiscent of the density of states of liquid water,[36] a feature also established in Raman scattering experiments.[14] Only the LDA structure shows a more detailed inelastic profile which could be termed remnant of the response of the crystalline

phases ice I_c and ice I_h.[2,20,25,26,46,47] There is an appreciable number of publications from IINS experiments[2,4–7] dedicated to the study of HDA dynamics. Indeed, some of the inelastic responses reported are in full or partial conformity with the results obtained here on ice XII rather than on HDA.

ACKNOWLEDGMENTS

The Rutherford Appleton Laboratory and the European Synchrotron Radiation Facility are thanked for the access to neutron and x-ray beam facilities.

[1] V. Petrenko and R. Whitworth, *Physics of Ice* (Oxford University Press, Oxford, 1999).
[2] D. D. Klug, E. Whalley, E. C. Svensson, J. H. Root, and V. F. Sears, Phys. Rev. B **44**, 841 (1991).
[3] J. Li, J. Londono, D. Ross, J. Tomkinson, and W. Sherman, J. Chem. Phys. **94**, 6770 (1991).
[4] A. Kolesnikov, V. Sinitsyn, E. Ponyatovsky, I. Natkaniec, and L. Smirnov, J. Phys.: Condens. Matter **6**, 375 (1994).
[5] J. Li, J. Chem. Phys. **105**, 6733 (1996).
[6] A. Kolesnikov, V. Sinitsyn, E. Ponyatovsky, I. Natkaniec, L. Smirnov, and J. Li, J. Phys. Chem. B **101**, 6082 (1997).
[7] A. I. Kolesnikov, J. Li, S. F. Parker, R. S. Eccleston, and C.-K. Loong, Phys. Rev. B **59**, 3569 (1999).
[8] P. V. Hobbs, *Ice Physics* (Clarendon, Oxford, 1974).
[9] C. Lobban, J. Finney, and W. Kuhs, Nature (London) **391**, 268 (1998).
[10] M. O'Keeffe, Nature (London) **392**, 879 (1998).
[11] M. Koza, H. Schober, A. Toelle, F. Fujara, and T. Hansen, Nature (London) **397**, 660 (1999).
[12] M. M. Koza, H. Schober, B. Geil, M. Lorenzen, and H. Requardt, Phys. Rev. B **69**, 024204 (2004).
[13] C. Salzmann, I. Kohl, T. Loerting, E. Mayer, and A. Hallbrucker, J. Phys. Chem. B **106**, 1 (2002).
[14] Y. Yoshimura, S. Stewart, H. Mao, and R. Hemley, J. Chem. Phys. **126**, 174505 (2007).
[15] B. Geil, M. M. Koza, F. Fujara, H. Schober, and F. Natali, Phys. Chem. Chem. Phys. **6**, 677 (2004).
[16] M. M. Koza, B. Geil, H. Schober, and F. Natali, Phys. Chem. Chem. Phys. **7**, 1423 (2005).
[17] M. Krisch and F. Sette, Top. Appl. Phys. **108**, 317 (2007).
[18] M. M. Koza, H. Schober, T. Hansen, A. Tolle, and F. Fujara, Phys. Rev. Lett. **84**, 4112 (2000).
[19] O. Mishima, L. D. Calvert, and E. Whalley, Nature (London) **310**, 393 (1984).
[20] H. Schober, M. M. Koza, A. Tolle, C. Masciovecchio, F. Sette, and F. Fujara, Phys. Rev. Lett. **85**, 4100 (2000).
[21] V. Sears, Neutron News **3**, 26 (1992).
[22] Y. P. Handa, O. Mishima, and E. Whalley, J. Chem. Phys. **84**, 2766 (1986).
[23] M. M. Koza, H. Schober, H. E. Fischer, T. Hansen, and F. Fujara, J. Phys.: Condens. Matter **15**, 321 (2003).
[24] M. Scheuermann, B. Geil, K. Winkel, and F. Fujara, J. Chem. Phys. **124**, 224503 (2006).
[25] H. Schober, M. M. Koza, A. Toelle, F. Fujara, C. A. Angell, and R. Boehmer, Physica B **241-243**, 897 (1998).
[26] M. M. Koza, B. Geil, K. Winkel, C. Kohler, F. Czeschka, M. Scheuermann, H. Schober, and T. Hansen, Phys. Rev. Lett. **94**, 125506 (2005).
[27] I. Kohl, E. Mayer, and A. Hallbrucker, J. Phys. Chem. B **104**, 12102 (2000).
[28] C. G. Salzmann, I. Kohl, T. Loerting, E. Mayer, and A. Hallbrucker, Phys. Chem. Chem. Phys. **5**, 3507 (2003).
[29] M. Koza, T. Hansen, R. May, and H. Schober, J. Non-Cryst. Solids **352**, 4988 (2006).
[30] S. Lovesey, *Theory of Neutron Scattering from Condensed Matter* (Oxford Science, Oxford, 1984).
[31] G. Squires, *Introduction to the Theory of Thermal Neutron Scattering* (Dover, Mineola, NY, 1996).
[32] H. Prask, H. Boutin, and S. Yip, J. Chem. Phys. **48**, 3367 (1968).
[33] H. Prask, S. Trevino, J. Gault, and K. Logan, J. Chem. Phys. **56**, 3217 (1972).
[34] B. Renker, *Physics and Chemistry of Ice* (Royal Society of Canada, Ottawa, 1973).
[35] G. Ruocco and F. Sette, J. Phys.: Condens. Matter **11**, R259 (1999).
[36] M. C. Bellissent-Funel, S. H. Chen, and J. M. Zanotti, Phys. Rev. E **51**, 4558 (1995).
[37] M. Bredov, B. Korov, N. Okuneva, V. Oskotskii, and A. Shakh-Budagov, Sov. Phys. Solid State **9**, 214 (1967).
[38] V. Oskotskii, Sov. Phys. Solid State **9**, 420 (1967).
[39] S. N. Taraskin and S. R. Elliott, Phys. Rev. B **55**, 117 (1997).
[40] N. Ashcroft and N. Mermin, *Solid State Physics* (Saunders, Philadelphia, 1976).
[41] R. Gagnon, H. Kiefte, and M. Clouter, J. Chem. Phys. **92**, 1909 (1990).
[42] C. Tulk, H. Kiefte, M. Clouter, and R. Gagnon, J. Phys. Chem. B **101**, 6154 (1997).
[43] L. Bosio, G. P. Johari, and J. Teixeira, Phys. Rev. Lett. **56**, 460 (1986).
[44] A. Bizid, L. Bosio, A. Defrain, and M. Oumezzine, J. Chem. Phys. **87**, 2225 (1987).
[45] M.-C. Bellissent-Funel, J. Teixeira, and L. Bosio, J. Chem. Phys. **87**, 2231 (1987).
[46] A. I. Kolesnikov, J. C. Li, S. Dong, I. F. Bailey, R. S. Eccleston, W. Hahn, and S. F. Parker, Phys. Rev. Lett. **79**, 1869 (1997).
[47] O. Yamamuro, Y. Madokoro, H. Yamasaki, T. Matsuo, I. Tsukushi, and K. Takeda, J. Chem. Phys. **115**, 9808 (2001).
[48] An example of a basic selection rule is the insensitivity of IXS and CINS to phonons of transverse polarization in the first Brillouin zone of high symmetry cubic crystals.